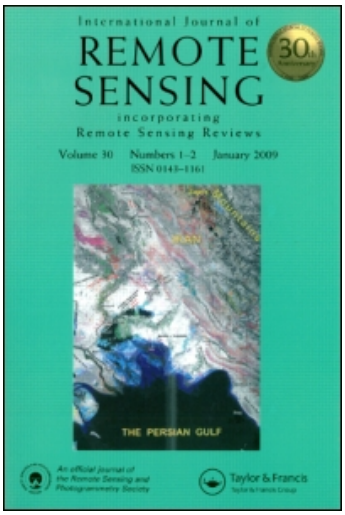

International Journal of Remote Sensing
Publication details, including instructions for authors and subscription information:
http://www.informaworld.com/smpp/title~content=t713722504

Improving the discrimination of vegetation and landform patterns in sandy rangelands: a synergistic approach

P. D. Blanco [a]; G. I. Metternicht [b]; H. F. Del Valle [a]
[a] Centro Nacional Patagónico CONICET, Puerto Madryn, Chubut, U9120ACV, Argentina [b] Division of Early Warning and Assessment, United Nations Environment Programme, Office for Latin America and the Caribbean, Clayton, Avenida Morse, Building 103, City of Knowledge, Panama City, Panama

Online Publication Date: 01 January 2009

To cite this Article Blanco, P. D., Metternicht, G. I. and Del Valle, H. F.(2009)'Improving the discrimination of vegetation and landform patterns in sandy rangelands: a synergistic approach',International Journal of Remote Sensing,30:10,2579 — 2605
To link to this Article: DOI: 10.1080/01431160802552785
URL: http://dx.doi.org/10.1080/01431160802552785

International Journal of Remote Sensing
Vol. 30, No. 10, 20 May 2009, 2579–2605

Taylor & Francis
Taylor & Francis Group

Improving the discrimination of vegetation and landform patterns in sandy rangelands: a synergistic approach

P. D. BLANCO*†, G. I. METTERNICHT‡ and H. F. DEL VALLE†
†Centro Nacional Patagónico CONICET, Boulevard Brown 3600, Puerto Madryn, Chubut, U9120ACV, Argentina
‡Division of Early Warning and Assessment, United Nations Environment Programme, Office for Latin America and the Caribbean, Clayton, Avenida Morse, Building 103, City of Knowledge, Panama City, Panama

(*Received 26 October 2007; in final form 3 March 2008*)

Soil erosion is a key factor in land degradation processes in the sandy rangelands of the Peninsula Valdés of Patagonia, Argentina. Mapping landform and vegetation patterns is important for improving prediction, monitoring and planning of areas threatened by sand and shrub encroachment. This paper investigates the contribution of optical sensors, such as the Terra Advanced Spaceborne Thermal Emission and Reflection Radiometer (ASTER), and textural measures derived from microwave Radarsat Advanced Synthetic Aperture Radar (ASAR) to their discrimination. An evaluation is undertaken to compare the classification accuracy achieved by specific regions of the spectrum and their synergistic use in an object-oriented approach. Image segmentation and object-oriented classifications were applied to the datasets. This required defining appropriate fuzzy membership functions for characterizing active and stabilized lineal dunes and the main vegetation classes. Improvements in the discrimination of active and stabilized dunes (vegetated by either scrub or grass) were achieved by using an object-oriented classification that integrated microwave and visible near-infrared (NIR) data. Changes in surface roughness caused by different vegetation types stabilizing the dunes affected the radar backscattering. Whereas Radarsat enabled a clear separation of scrub-stabilized dunes, Terra-ASTER showed superior performance in the cartography of grass-stabilized dunes. The synergistic use of microwave and visible and near-infrared (VNIR) data yielded a substantial increase in the discrimination and mapping of landform/vegetation patterns.

1. Introduction

1.1 *Criteria for mapping rangelands*

Arid and semiarid drylands encompass nearly one-third of the world's land surface (OIES 1991). Among these, rangelands are essential contributors to the productivity and biodiversity of the biosphere as they support the global population of domesticated livestock and represent a key component of global ecosystem function and biodiversity (Stafford Smith 1996). It is estimated that between 50% and 70% of the world's rangelands are degraded as a result of overgrazing, aggravated by the characteristics of dryland climates (Warren and Agnew 1988). Long-term major

*Corresponding author. Email: blanco@cenpat.edu.ar

International Journal of Remote Sensing
ISSN 0143-1161 print/ISSN 1366-5901 online
http://www.tandf.co.uk/journals
DOI: 10.1080/01431160802552785

effects of grazing, such as an increase in bare soil exposed to erosive effects and encroachment of unpalatable woody plants, are well documented (Schlesinger *et al.* 1990, Bahre and Shelton 1993, Milchunas and Lauenroth 1993, Perkins and Thomas 1993).

Sandy rangelands with wind-erodible soils and low resilience are particularly vulnerable to the consequences of land degradation (Warren and Agnew 1988). Wind erosion and heavy grazing are the principal mechanisms of land degradation in sandy rangelands (Okin *et al.* 2001). Once soil is exposed by heavy grazing, wind erosion occurs immediately (Whitford *et al.* 1995). Generation of active sand dunes, expansion of sand-seas and reactivation of stabilized dunes are major manifestations of wind erosion in these environments (Le Houérou 1993).

Establishing criteria for accurate mapping of arid and semiarid regions in general, and sandy rangelands in particular, facilitates identifying locations where different degradation processes dominate. Detecting either increased sand cover or greater woody biomass is an important contribution to identifying sites that are experiencing changes that can be described as land degradation. As not all sites are equally vulnerable to degradation, it is of value to know the spatial distribution of vegetation and landform patterns in an integrated (phyto-geomorphological) manner, to identify areas prone to erosion, so that appropriate conservation and management measures can be implemented.

1.2 *Background and objectives*

Satellite remote sensing is an effective tool that can be used for mapping sandy rangelands in a rapid and accurate manner over large areas. Previous research on the use of passive and active spaceborne sensors for mapping sandy rangeland patterns of degradation, as well as image processing techniques adopted to this end, are summarized below.

Ground- and satellite-based research shows that visible-infrared (VIR) data can be used to discriminate vegetation and landform patterns based on the distinctive reflectance values of light-coloured sands (property of active dune areas) and dark-coloured vegetation, which produce significant tonal differences (e.g. Paisley *et al.* 1991, Tucker *et al.* 1991, 1994, Sanjeevi 1996, Kutiel *et al.* 2004, Ballantine *et al.* 2005). However, image processing techniques based purely on spectral information of the VIR region present limitations for distinguishing between vegetation types given the saturation of the observed signal with increasing biomass (Palmer and van Rooyen 1998).

However, data collected using Synthetic Aperture Radar (SAR) have the potential to provide information on the geometry of sand dunes and other aeolian features because of the sensor's susceptibility to changes in the structure of surface features. This is particularly important in areas where dunes are not pronounced and, as a consequence, optical remote sensors may fail to reveal the dunes' geometry. Previous research has shown that SAR imagery can also provide useful information for distinguishing stable vegetated areas from bare areas of active sand dunes (Blom and Elachi 1981, Lancaster *et al.* 1992, Greeley and Blumberg 1995, Blumberg 1998, del Valle and Blanco 2006). These studies consistently indicate that the visibility of sand dunes on radar images is a function of wavelength, incidence angle and polarization characteristics of the sensor. However, most of the current radar spaceborne systems only collect data at a single wavelength with a fixed polarization. Future systems will include an increased number of wavelengths and

polarizations, but until such time the goal of increased informational content may be reached through simpler methods, such as the extraction of textural measures, as discussed below.

The textural component of ground targets provided by active microwave data has the potential to furnish additional information for mapping land features (Herold *et al.* 2004). As the information content of a radar image resides in both the intensity (spectral) of individual pixels and the spatial arrangement of those pixels, the textural information that can be derived from such imagery can be as valuable as information derived from the visible and near-infrared (VNIR) (Anys and He 1995). Characterization of areas on the basis of a range of radar-derived textural measures has been used successfully for mapping shrub encroachment (Hudak and Wessman 1998, 2001, Shupe and Marsh 2004), to discriminate landforms (Frohn *et al.* 2005, Drăgut and Blaschke 2006), and also for various land-use/land-cover mapping projects (van der Sanden and Hoekman 1999, Haack and Bechdol 2000).

Furthermore, pixel-based classifications are generally unsatisfactory for rangelands, which often consist of highly variable mixtures of scattering objects and are largely distinguished by their spatial, as well as their spectral, characteristics (Blumberg 1998). Schiewe *et al.* (2001) report that traditional algorithms such as the maximum likelihood classification produce too many or ill-defined classes. Object-based segmentation and image classification techniques are receiving increasing attention for classification of spectral and SAR data because these techniques account for relationships between adjacent pixels, including shape, texture, relational and contextual information. The synergy of this information enables mapping of individual objects as opposed to single pixels (Thomas *et al.* 2003). In addition, from an ecological perspective, it is more appropriate to analyse objects, as opposed to pixels, because landscapes consist of patches that can be detected in the imagery using object-based analysis. Pixels are aggregated into image objects by segmentation, which is defined as the division of remotely sensed images into discrete regions or objects that are homogeneous with regard to spatial or spectral characteristics (Ryherd and Woodcock 1996).

The current study focused on the cartography of vegetation and landforms over a sandy rangeland by combining multiresolution image segmentation and object-oriented image classifications of VNIR and microwave satellite data. The three primary objectives of the study were: (1) to assess whether information content can be increased by specific SAR enhancements, and select optimal textural measures for the discrimination of vegetation and landforms, (2) to investigate and implement object-oriented image analysis algorithms and fuzzy logic techniques for the recognition and classification of vegetation and landforms from radar-derived textural measures and VNIR data, and (3) to assess the effect that the synergy of textural and optical data exerts on the classification accuracy of vegetation and landforms of sandy rangelands. We hypothesized that the synergistic use of data from these discrete portions of the electromagnetic spectrum could be used for accurate and economic mapping of vegetation and landforms in sandy rangelands.

The sandy rangelands at the Peninsula Valdés, located in Patagonia, Argentina were selected because of the presence of spatial patterns related to soil degradation processes. Dunes in this area were formed in the upper Pleistocene from loose, sand-sized sediment of the sandy beaches and cliffs exposed to the prevalent westerly winds (Beltramone *et al.* 1993). Nowadays, dunes are mostly stabilized by vegetation, with some active sand dunes, grouped in discrete megapatches of

different ages, that are moving at different distances from the western coast where they were generated (Súnico 1996). This system is extremely fragile and subject to soil degradation by wind and overgrazing. By assessing the spatial pattern and extent of vegetation and landforms, this work aimed to provide information that can be significant for prediction and monitoring of areas threatened by sand and shrub encroachment in this region.

2. Methods

2.1 *Study area*

This research was conducted in an area of about 300 km^2 centred at 42°32′ S, 63°54′ W in Peninsula Valdés (southern Patagonian Monte, Argentina). The climate is semiarid, characterized by an annual mean temperature of 13°C and an average annual rainfall (1912–2002) of 231 mm, with a high mean interannual variation (coefficient of variation 30%; Barros and Rivero 1982). The prevailing winds are from the west and northwest (Coronato 1994). The mean annual wind speed is 25 $km\,h^{-1}$ (Barros *et al.* 1981). The area is strongly influenced by intense winds from the northeasterly direction prevailing from October to February (Labraga 1994).

The study area is flat, with a modest undulating relief dominated by aeolian sands. Landforms mostly result from wind erosion and sand deposition. Two dunefields are distinguishable in Peninsula Valdés: the largest one is in the central area, forming a belt that stretches from the west to the east coast, and the smaller one is a fringe-like dunefield located in the southwest corner of the peninsula. Two main generations of dunes can be identified in the dunefields: (1) megapatches of active dunes, including a series of aeolian forms such as barchan, dome and transverse dunes, and (2) relict aeolian landforms, including vegetated sand sheets and stabilized lineal dunes on several alignments, that are not in accord with present wind regimes (Beltramone *et al.* 1993). Active dunes are about 20 m height and the average rate of dune movement has been measured at 9.1 ± 3.7 m $year^{-1}$ (del Valle *et al.* 2007). Associated with the active dunes, there are deflationary surfaces, namely regs, where aeolian activity has removed fine particles leaving lag gravels. Lineal dunes are about 10 m high, trending in a WNW–ESE direction.

The vegetation covers 50–80% of the dunefields and the most widespread communities stabilizing sand are grasslands, with palatable, annual and perennial grasses (the dominant species are *Sporobolus rigens*, *Panicum urvilleanum* and *Stipa tenuis*), and scrublands dominated by *Hyalis argentea*, an unpalatable, perennial scrub (or sub-shrub) forming large, dense homogeneous stands as shown in figure 1 (Bertiller *et al.* 1981). Historically, most of the area was dry grassland, but shrub encroachment by *Hyalis argentea* has led to the conversion of much of the area to shrubland. A shrub steppe of *Chuquiraga avellanedae* extends between both dunefields, but this area was excluded from this study. Pastoralism, especially sheep grazing, has been the major land use over the past 100 years (Defossé *et al.* 1992).

Based on pre-existing physiographic and vegetation maps (Bertiller *et al.* 1981, Sunico 1996) and observations of the actual situation in the field, six dominant vegetation/landform patterns were identified in the study area. These are: Active Dune, Reg, Grassland, Grass Stabilized Lineal Dune, Scrubland, and Scrub Stabilized Lineal Dune.

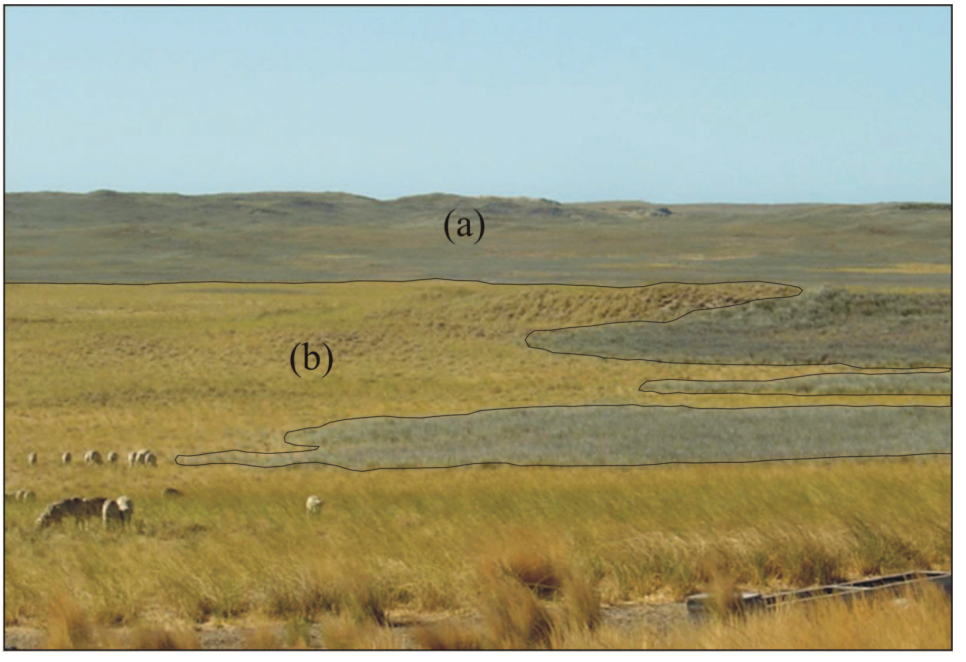

Figure 1. Ground photograph of dunefields vegetation communities: (*a*) scrubland dominated by *Hyalis argentea*, with stabilized lineal dunes in the background, and (*b*) grassland dominated by *Sporobolus rigens*, *Panicum urvilleanum* and *Stipa tenuis*.

2.2 *Remotely sensed data*

2.2.1 Optical data. An Advanced Spaceborne Thermal Emission and Reflection Radiometer (ASTER) level 1B scene (raw product corrected for instrumental and geometric errors; ERSDAC 2000) was acquired over the study area. The Terra-ASTER sensor acquires data in three separate subsystems: VNIR (bands 1, 2 and 3, spatial resolution of 15 m), shortwave infrared (SWIR; bands 4–10, spatial resolution of 30 m), and thermal infrared (TIR; bands 11–14, spatial resolution of 90 m). The image was acquired on 27 November 2004, georeferenced in the Universal Transverse Mercator projection (UTM Zone 20), WGS-84 ellipsoid, and converted to radiance values.

Given the high correlation between the ASTER bands (above 0.9), a principal component analysis (PCA) was applied to remove redundant information. The analysis revealed that the first two components explained 98% of the image variability, and thus they were selected for further analysis. The ASTER bands 1, 2, 3 and 4 showed the highest contribution to these first two components (figure 2), and thus were selected as the raw bands to be included in the classification process.

The Soil Adjusted Vegetation Index (SAVI), designed to minimize the effect of the soil background (Huete 1988), was applied to the ASTER data as a means to gather information on vegetation cover. Similarly to the Normalized Difference Vegetation Index (NDVI), the NIR and red bands are used in the calculation of the SAVI, but with the addition of an adjustment factor (L) that varies between 0 and 1. We used an adjustment factor of 0.5, which has been shown to reduce soil influences considerably (Huete 1988) and is the most widely used adjustment factor for intermediate vegetation cover.

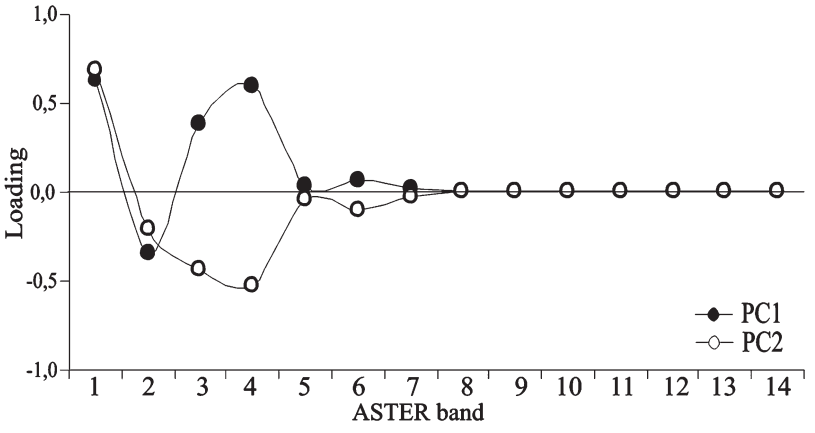

Figure 2. Contribution of each ASTER band in the first two components of the PCA.

2.2.2 SAR data. The SAR sensor onboard Radarsat collects data in the C-band (5.6 cm wavelength), with a single horizontal–horizontal (HH) polarization. The image of the study area was acquired in fine mode 4, mode descending (west looking) at an incidence angle of 44°, with a nominal spatial resolution of 8 m. A Radarsat-1 SAR image acquired on 1 January 2005 was used to evaluate the contribution of the microwave region of the spectrum to the differentiation of vegetation/landforms in the study area. Radar surface feature interaction, or scattering, and the characteristics of this scattered energy, or backscatter, are mainly sensitive to four parameters: target orientation, surface roughness, volumetric inhomogeneities and the dielectric constant of the target material (Elachi *et al.* 1982, Ford *et al.* 1989, Blumberg 1998). Although the dielectric constant is sensitive to variations in water content, the low soil moisture of desert areas increases the importance of the other parameters in energy backscatter (Sano *et al.* 1998).

Radarsat data were received in raw signal format and subsequently converted to magnitude image products (ERDAS Inc. 2003). To decrease the speckle contribution, different low-pass filter treatments were tested. The variations in parameters for each low-pass spatial filtering treatment were window size, number of iterations, the algorithm used (γ-MAP, Lee-Sigma, Local Region, Frost, and Median), the coefficient of variation (for γ-MAP and Lee-Sigma filters) and the number of standard deviations (for the Lee-Sigma filter). Evaluation of the filtering treatments was based on quantitative and visual assessment of the edge-boundary preservation and the decrease of the 'granular' aspect of the radar image. The speckle index (Lee and Jurkevich 1994) was selected as the quantitative parameter to evaluate filter performance. A low speckle index indicates a good ability of the filter to reduce the noise on the image. The more effective filtering treatment was three iterations of the Frost filter with square window sizes of three, three and five pixels, respectively. The speckle index decreased from 1.58 for the raw Radarsat scene to 0.63 for the filtered image. The filtered image was geocoded in the UTM projection Zone 20.

2.3 *Extraction of Radarsat-derived textural measures*

Among the existing methods of texture representation, the best known are statistical transformations (Hsu 1978), the Fourier power spectrum method (Weska *et al.* 1976) and the Haralick grey level co-occurrence (GLC) matrix method (Haralick

et al. 1973). The GLC procedure is by far the most widely used approach for computing second-order texture measures (Haralick 1979, Karathanassi *et al.* 2000, Treitz and Howarth 2000), and thus we restricted our study to this method to ascertain their relative value in mapping vegetation and landform patterns. The goal of the co-occurrence matrix method is also, as in the normal texture analysis, to describe the grey value relationships in the neighbourhood of the current pixel. However, the grey value relationships are analysed in the co-occurrence matrix space and not using the original grey values. In the transformation from the image space into the co-occurrence matrix space, only the neighbouring pixels in one or some of the eight defined directions are used.

Haralick *et al.* (1973) proposed 14 statistical features calculated on the GLC matrix for extracting textural information. Among these features, and in a similar way to previous studies (Ulaby *et al.* 1986, Kurvonen and Hallikainen 1999, Narasimha Rao *et al.* 2002), we selected the mean, variance, homogeneity, contrast, dissimilarity, entropy, angular second moment, and correlation measure. These textural features are described briefly in table 1.

Table 1. Image texture measures derived from the SAR image.

Texture measure	Description	Equation*
Mean	Mean is the average grey level for each sample	$\sum_{i,j=0}^{N-1} i(P_{i,j})$
Variance	Variance is a measure of heterogeneity; it increases when the grey level values differ from their mean. In general, coarse-textured features are associated with higher variances	$\sum_{i,j=0}^{N-1} P_{i,j}(i-\mu_i)^2$
Homogeneity	This parameter measures image homogeneity as it assumes larger values for smaller grey tone differences in pair elements	$\sum_{i,j=0.}^{N-1} \frac{P_{i,j}}{1+(i-j)^2}$
Contrast	Contrast is a measure of spatial frequency, the difference between the highest and the lowest values of a contiguous set of pixels. A high contrast implies high coarse texture	$\sum_{i,j=0}^{N-1} P_{i,j}(i-j)^2$
Dissimilarity	Dissimilarity, akin to contrast, describes the heterogeneity of the grey levels. Higher values of dissimilarity in the GLC matrix indicate coarser textures	$\sum_{i,j=0}^{N-1} P_{i,j}\lvert i-j\rvert$
Entropy	Entropy measures the disorder of an image. When the image is not texturally uniform, many GLC matrix elements have very small values, which imply that entropy is very large	$\sum_{i,j=0}^{N-1} P_{i,j}(-\ln p_{i,j})^2$
Angular second moment	This parameter measures textural uniformity. Thus, high angular second moment values occur when the grey level distribution over the window has either a constant or a periodic form	$\sum_{i,j=0}^{N-1} {P_{i,j}}^2$
Correlation	Correlation is a measure of grey-tone linear dependencies in the image. High correlation values imply a linear relationship between the grey levels of pixel pairs	$\sum_{i,j=0}^{N-1} P_{i,j}\left[\frac{(i-\mu_i)(j-\mu_j)}{\sqrt{(\mathrm{SD}_i^2)(\mathrm{SD}_j^2)}}\right]$

From (i, j=0) to ($N-1$), each cell in the co-occurrence matrix is considered; i, row number; j, column number; μ, mean; SD, standard deviation; $P_{i,j}$, probability value from the co-occurrence matrix.

*Source: Hall-Beyer (2004).

The GLC matrix depends on (i) the number of grey levels, (ii) the distance between pixels and (iii) the direction ($0^\circ, +45^\circ, +90^\circ, +135^\circ$) for each of Haralick's textural features. Despite an increase in computation time, the number of grey levels was set to 256 to avoid losing information. The choice of an adequate distance between pixels is closely related to the coarseness or the fineness of the texture in the image to be processed. Hence, interpixel distances (IPDs) of 1, 3, 5, 7, 9 and 11 (valid for both fine and coarse textures) were evaluated. Finally, considering the randomness of orientation of natural features, a GLC matrix computed in all directions was considered appropriate. In view of the predominant west–east orientation of landforms in the study area, and assuming the redundancy of texture in different orthogonal directions, the GLC matrix was generated at a single direction angle of 90°.

Texture features should be able to discriminate clearly between different textures, while presenting little variability inside each class. Therefore, to evaluate the performance of each of the textural measures and to identify the best performing set, the following procedure was applied: (1) image segments of 30×30 pixels each, representing textural patterns of the classes of interest, were identified in the Radarsat image; (2) the texture of these features was computed and normalized linearly for all the segments to enable comparative evaluation of each feature; (3) scatter plots of the normalized values as a function of IPDs were produced for all textural measures; and (4) the selection of textural features was made based on the discrimination capability of the different classes.

2.4 *Image data integration*

An image-to-image registration was conducted between the ASTER and the Radarsat images to keep registration errors to less than half a pixel. As the study area presents an almost flat topography, a first-order polynomial transformation and nearest-neighbour resampling were used to create the output images with a common resolution of 8 m. Bands 1–4 from ASTER and the selected Radarsat-derived texture measures were stacked into one single image in Erdas 8.7 (ERDAS Inc. 2003).

2.5 *Object-oriented approach*

An object-oriented multiscale image analysis method embedded in the software eCognition (Baatz and Schaepe 2000, Definiens 2003) was used. Figure 3 shows the conceptual model designed for an object-oriented classification of the ASTER- and Radarsat-derived dataset. The approach can be divided into two major parts. First, multiresolution segmentation of the remotely sensed data is performed. This procedure is analogous to a visual interpretation and can be done at various scales. The outputs are highly homogeneous segments at an adequate scale and of a comparable size. Once segmentation is complete, classification is performed using those objects rather than single pixels. The classification of the image objects can be performed by using a nearest-neighbour classifier based on user-selected samples or by developing fuzzy membership functions based on fuzzy logic theory combined with user-defined rules. A fuzzy membership function ranges from 0 to 1 for each object's feature values with regard to the object's assigned class. Spectral, shape and statistical characteristics as well as relationships between linked levels of the image objects can be used in the rule base to combine objects into meaningful classes (Benz *et al.* 2004).

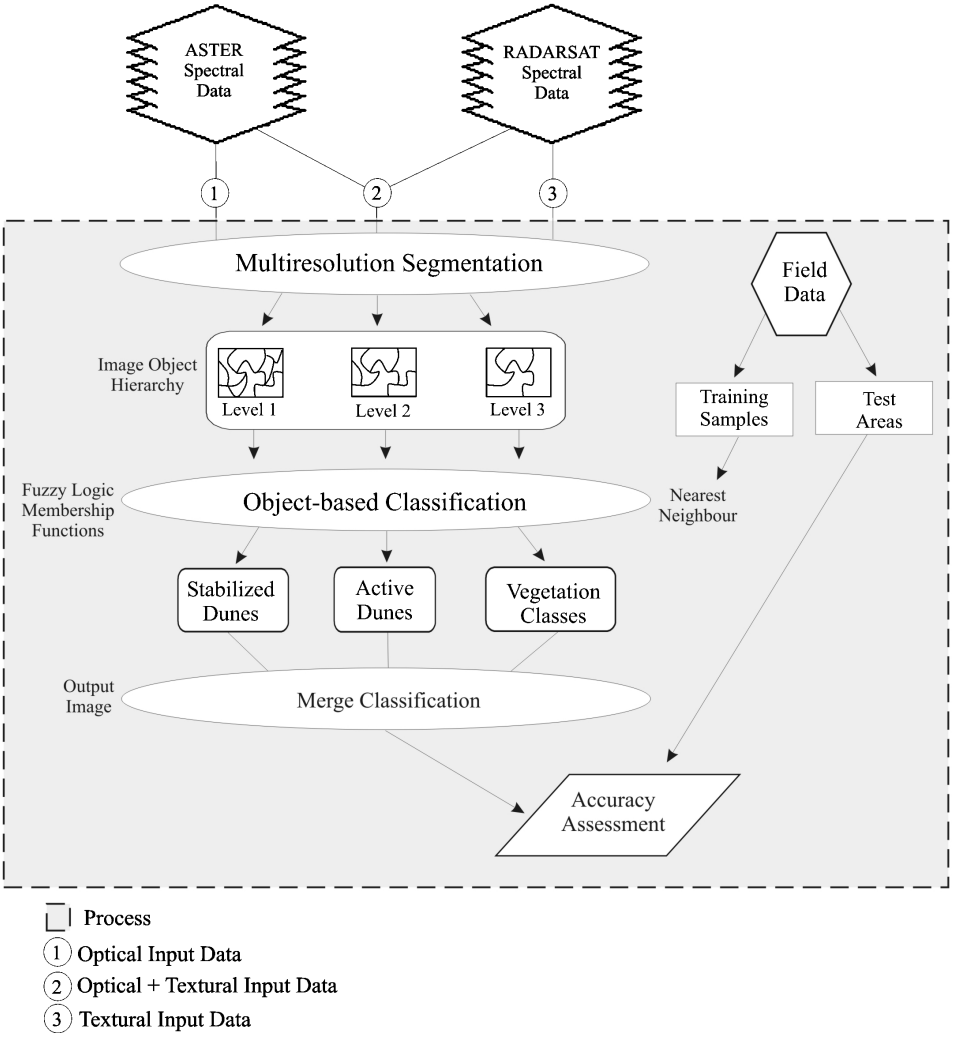

Figure 3. Conceptual model of the object-oriented approach adopted.

2.5.1 Segmentation. Three projects were implemented in this research using different input datasets (table 2). The first project used the VNIR and SWIR bands of ASTER (e.g. bands 1–4) as data input for image segmentation and classification. The second project included the co-occurrence texture images derived from the Radarsat data. The third project segmented and classified a dataset of integrated optical and textural measures. All projects included the SAVI image as well.

Table 2. Scale parameters considered for each project.

		Scale		
Project	Dataset used	Level 1	Level 2	Level 3
1	B1–4 ASTER	3	7	9
2	Textural measures	8	15	25
3	ASTER combined texture	8	15	25

The object-oriented approach considers three parameters for image segmentation, namely scale, colour/shape ratio and form/spatial properties (smoothness/compactness ratio) (Baatz *et al.* 2004), where colour and shape parameters can be weighted from 0 to 1. The most suitable scale parameter, that is the one giving the smallest possible number of objects while keeping homogeneity in terms of the targeted class, was selected at each level. Therefore, broad land-cover types (vegetation types, not-vegetated areas) can be defined at coarser scales, whereas medium scale discriminates active dunes, and a finer scale identifies stabilized lineal dunes. The segmentation weights for colour and shape was established after several iterations to a ratio of 0.8 : 0.2 for the relative importance of reflectance *versus* shape, and 0.1 : 0.9 for compactness *versus* smoothness.

2.5.2 Object-oriented classification. The image classification steps are described next and are shown in the flowchart of figure 4. The highest hierarchical level, which was segmented on the coarser scale, was classified using a SAVI threshold. Those objects whose SAVI value was below 0.74 were considered to be *Dunefield*, and those whose SAVI values were above 0.74 were classed as *Scrubland*. The selection of 0.74 was empirical, based on an inspection of the image objects within the study area. This initial step was necessary to mask out the *Shrub Steppe* from the remaining classification scheme. At the same level, the *Dunefield* was classified into *Grassland*, *Scrubland* and *Areas Not Vegetated*. These classes were identified and separated by selecting an appropriate training set of object features chosen in the SAVI feature space. A nearest-neighbour classifier was then applied using the most significant differentiating objects for the three classes.

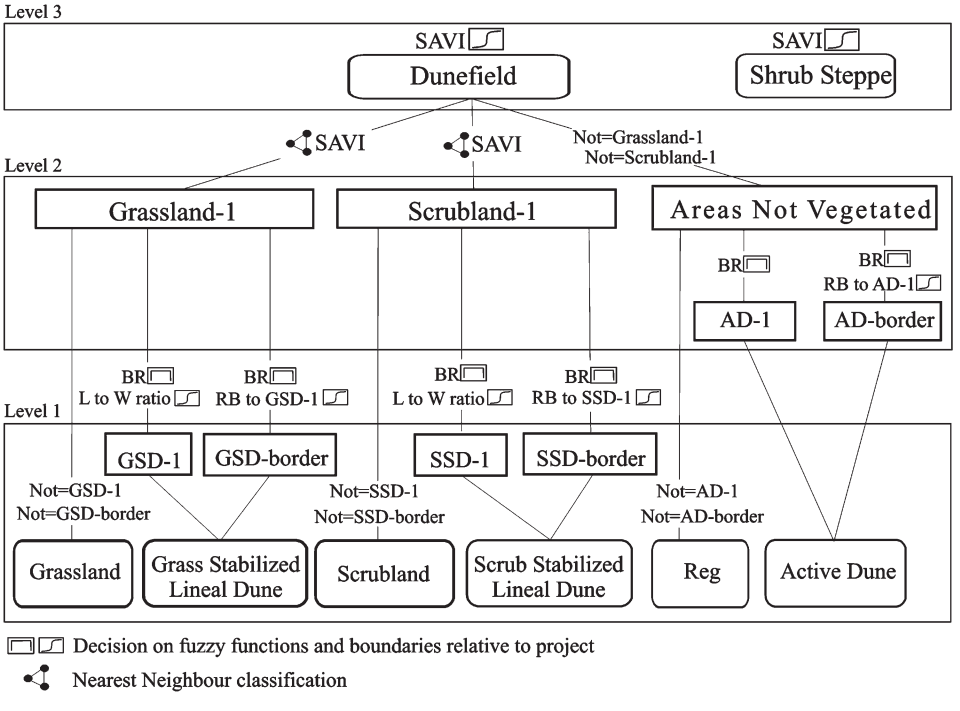

Figure 4. Fuzzy membership functions for all classes. AD, Active Dune; GSD, Grass Stabilized Lineal Dune; SSD, Scrub Stabilized Lineal Dune; BR, brightness; L, length; W, width; RB, the relationship of border to a certain class.

Table 3. Decision on brightness feature space and fuzzy boundaries.

	Brightness feature space		
Classes	B1–4 ASTER	Textural measures	ASTER combined texture
AD-1	27<BR<46	5<BR<22	25<BR<43
AD-border	24<BR<46	5<BR<33	25<BR<48
SSD-1	17<BR<19	44<BR<48	15<BR<16
SSD-border	17<BR<20	39<BR<56	14<BR<17
GSD-1	21<BR<22	33<BR<43	18<BR<20
GSD-border	20<BR<23	31<BR<48	18<BR<24

AD, Active Dune; GSD, Grass Stabilized Lineal Dune; SSD, Scrub Stabilized Lineal Dune; BR, brightness.

At the next lower level, the basic aim was to identify active dunes. This feature was therefore classified by defining fuzzy membership functions for mean brightness values, related to the input data for each project (table 3). Two subclasses of the *Active Dune* (*AD*) were defined, *AD-1* and *AD-border*, the latter with a feature space broader but a constraint of relative border length to *AD* greater than 0.5 imposed. Subsequently, an object fusion was applied to group the objects of these classes in the common class *AD*. The *Reg* class was defined as complementary to *AD*.

At the lowest hierarchical level, a classification was implemented for the extraction of stabilized dunes. We discriminated between dunes stabilized by grass and dunes fixed by scrub. Therefore, the classes *Grass Stabilized Lineal Dune (GSD)-1* and *Scrub Stabilized Lineal Dune (SSD)-1* were classified based on membership functions for mean brightness values. Because these classes had similar brightness values and could be confused with other classes, a restriction was established on the shape of the segments: that is the length/width ratio should be greater than 4. To account for wrongly excluded objects, two new subclasses were defined: *GSD-border* and *SSD-border*. These subclasses had the brightness feature space broader than *GSD-1* and *SSD-1*, respectively, but with the constraint that the relative border length to these classes was greater than 1. Lastly, a fusion of these classes was performed leading to the final extraction of the classes *Grass Stabilized Lineal Dune* and *Scrub Stabilized Lineal Dune*. The *Grassland* and *Scrubland* classes were defined as complementary to these classes, respectively.

2.6 *Validation*

Accuracy assessment was performed by means of an error matrix based on stratified and randomly selected sites across the study area, ensuring at least 50 samples per class (Story and Congalton 1986). Ground truthing was carried out by field survey in the summer of 2005, visiting as many sites as possible, and confirming the vegetation/landform type *in situ* with a Global Positioning System (GPS) unit. At each validation site, an area at 45 m by 45 m was examined to account for location errors caused by positional inaccuracies of the GPS and/or the geometric correction of the satellite imagery. The number of validation pixels was 729 for *Active Dune*, 414 for *Reg*, 369 for *Grassland*, 360 for *Scrubland*, and 837 and 792 for *Lineal Dunes Stabilized by Grass* and *Scrub*, respectively.

The error matrix was used as the basis for calculating the overall accuracy, and individual class user's and producer's accuracy (Congalton 1991). The KHAT statistic $\left(\hat{K}\right)$, which is an estimate of the kappa coefficient, and its variance were

also calculated to compare the accuracy of the classifications to that of a random pixel classification (Congalton and Green 1999). This method uses the normal curve deviate statistics Z given by:

$$z = \frac{\hat{k}}{\sqrt{\hat{\mathrm{var}}\left(\hat{k}\right)}} \tag{1}$$

where the denominator is the square root of the sample variance from $\hat{k}$.

2.7 *Efficiency of the synergistic approach*

This phase of the study aimed to assess the efficiency of combining synergistically ASTER and Radarsat sensor data for classification of vegetation/landforms. The efficiency of the synergic approach was evaluated from two points of view, the classification accuracy and the economic/financial cost of the satellite images.

2.7.1 Classification accuracy. The two maps obtained using information from a single sensor were compared with the map obtained when the optical data were combined with textural information. To this end, the KHAT statistic and its variance were used to construct a hypothesis test for statistically significant difference between error matrices (Cohen 1960). The null hypothesis is that there is no disagreement between the KHAT values:

$$z = \frac{\left|\hat{k}_1 - \hat{k}_2\right|}{\sqrt{\hat{\mathrm{var}}\left(\hat{\mathrm{k}}_1\right) + \hat{\mathrm{var}}\left(\hat{\mathrm{k}}_2\right)}} \tag{2}$$

where $\hat{k}_1$ and $\hat{k}_2$ are the two different KHAT statistics being compared, and the denominator is the square root of the sum of the sample variances from $\hat{k}_1$ and $\hat{k}_2$, respectively.

To determinate the degree of agreement and disagreement and the spatial distribution of the differences between maps, we used a fuzzy set approach proposed by Hagen-Zanker *et al.* (2005) as the Map Comparison KIT (MCK) software. The approach is aimed specifically at categorical raster maps, and it makes use of fuzzy set techniques to account for fuzziness of location and fuzziness of category, as defined in Hagen-Zanker *et al.* (2005). Fuzziness of location is taken into account by enabling the fuzzy representation of a cell to be partly defined by neighbouring cells. A function (e.g. exponential decay, linear decay or constant value) defines the level to which neighbouring cells exert this influence. Similarly, a category similarity matrix can be applied to highlight or disregard different types of similarity, and thus better characterize the fuzziness of categories. After different trials the category similarity matrix shown in table 4 was applied to account for fuzziness between the vegetation and landform patterns considered. For instance, this matrix considers that *Grassland* and *Grass Stabilized Lineal Dune* classes are more similar to each other than to *Reg* and *Active Dune* classes, but they are not considered so different from *Scrubland* and *Scrubland Stabilized Lineal Dunes*. Furthermore, after trying different values, a neighbourhood radius equal to 20 cells and a halving distance of 5 were applied as they showed the best comparison results. The result of comparing two maps is a third map, indicating for each cell the level of agreement in a range from 0 (low similarity) to 1 (identical) between categories.

Table 4. Fuzzy similarity matrix.

Class	AD	Reg	Grassland	GSD	Scrubland	SSD
AD	1	0.5	0	0	0	0
Reg	0.5	1	0	0	0	0
Grassland	0	0	1	0.6	0.4	0.4
GSD	0	0	0.6	1	0.4	0.4
Scrubland	0	0	0.4	0.4	1	0.6
SSD	0	0	0.4	0.4	0.6	1

AD, Active Dune; GSD, Grass Stabilized Lineal Dune; SSD, Scrub Stabilized Lineal Dune.

2.7.2 Economic/financial cost. We evaluated the efficiency of the synergistic approach in relation to the cost of the images used. Plot diagrams were built up to compare and evaluate the results of integrating different image data sources. The *x*-axis represents the overall and per class accuracies obtained by using a particular sensor or a combination of sensors, while the cost of the images used are plotted on the *y*-axis.

3. Discussion of results

3.1 *Optimization of Radarsat-derived texture measures*

Examination of figure 5, the Radarsat image for a portion of the study area, shows poor effectiveness for visual separation of vegetation/landforms in this region. Active dunes, acting almost as a specular surface to the radar signal, display a dark

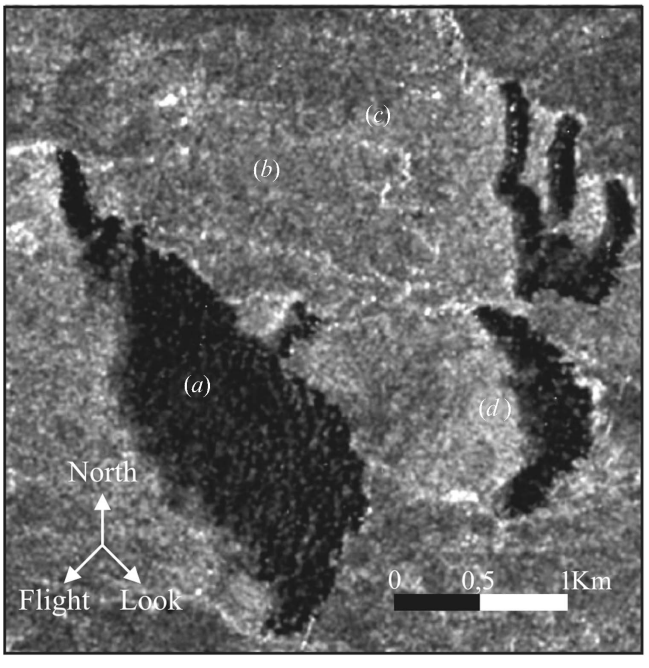

Figure 5. Radarsat-1 SAR, C-band HH polarization image showing part of the study area. The brightness tones represent higher backscatter magnitude values. The parts labelled (*a*) to (*d*) are described in the text.

tone due to the low backscatter (figure 5(*a*)). Natural vegetation has a strong backscatter, mainly controlled by volume scattering, providing uniform medium to bright grey tones (figure 5(*b*)). Grassland and scrubland areas cannot be separated visually in this scene. Within these lighter, vegetated regions are some isolated very high return features representing lineal dunes stabilized by vegetation (figure 5(*c*)). Rock fragments in erosion pavements presented a rough surface in the radar sense, and thus regs are seen as light grey due to high backscatter (figure 5(*d*)). Regs are not clearly identifiable because they produce a high backscatter similar to natural vegetation.

The confusion associated with the raw Radarsat's vegetation and landform backscattering suggest that measures of image texture might increase the discriminatory ability of the SAR image. In figure 6 we present the normalized means of the textural features for all the classes. The class *Active Dune* showed the finest texture reflected in the highest correlation and lowest contrast and variance. Natural vegetation presented coarser textures than *Reg* and *Stabilized Lineal Dune* classes, which had less variance, more contrast and dissimilarity. *Scrubland* showed coarser texture than grassland areas, this being evident in its larger dissimilarity. Comparison of the vegetation and landform patterns separable by the textural features clearly reveals that the tonal average is important because its sole use could

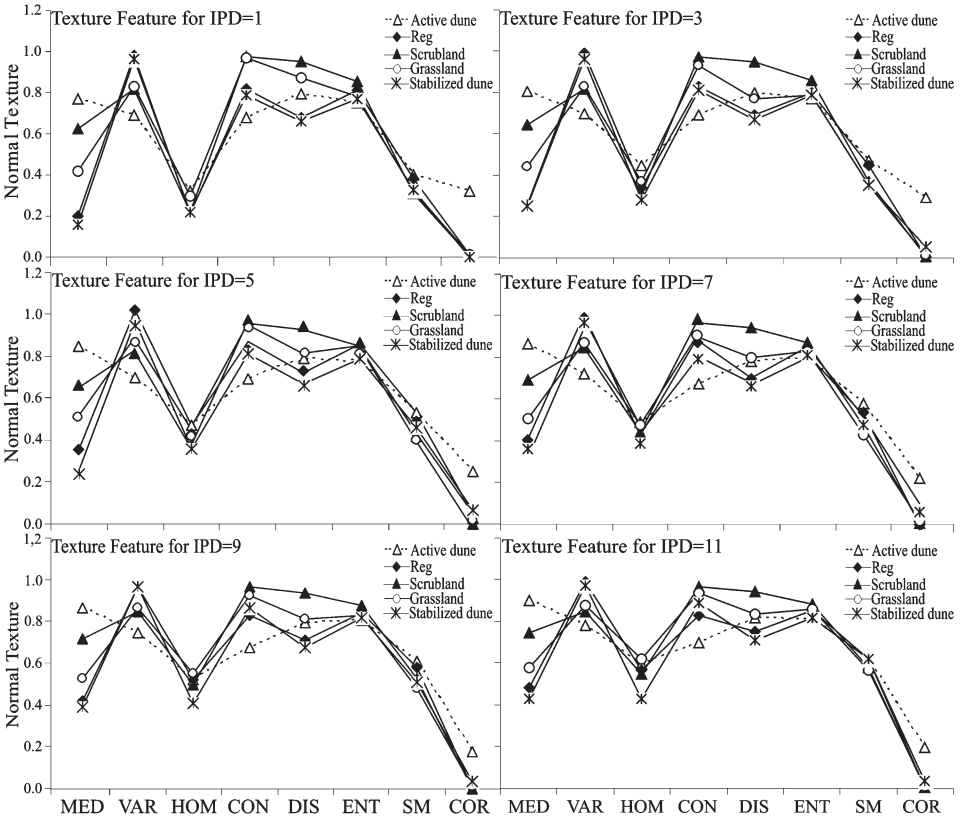

Figure 6. Capability of discriminating between texture patterns by GLCM texture features: MED, mean; VAR, variance; HOM, homogeneity; CON, contrast; DIS, dissimilarity; ENT, entropy; SM, angular second moment; COR, correlation.

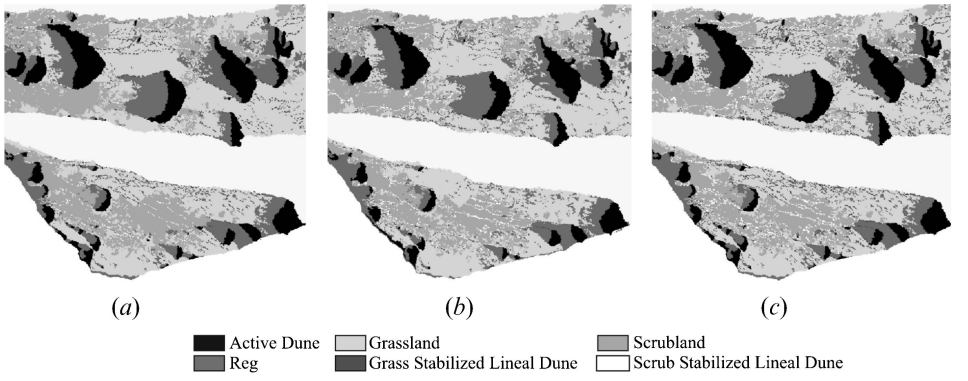

Figure 7. Object-oriented classifications based on optical data from ASTER (*a*), textural measures derived from Radarsat (*b*), and merged optical and texture image data (*c*).

exclusively discriminate all covers. Thus, the mean became the first choice among the textural features. *Reg* and *Stabilized Lineal Dune* classes were found to be discriminated by variance at IPD=5 and contrast at IPD=7, respectively. *Grassland* and *Scrubland* are well discriminated by dissimilarity at IPD=5. Hence, this textural feature was also selected as a complementary feature to mean, variance and contrast for discrimination of all the classes. Therefore, the mean, variance and dissimilarity images from the GLC matrix computed at IPD=5 and contrast image computed at IPD=7 were generated and used for further object-oriented classification.

3.2 *Vegetation and landform mapping*

The object-oriented classification outputs obtained from ASTER alone, textural information from Radarsat, and ASTER combined with the Radarsat texture dataset are shown in figure 7. The areal and proportional extent of vegetation and landform patterns resulting from the different layer input maps are summarized in table 5.

Differences in the extent of vegetated and non-vegetated areas have the strongest influence on the three classifications (approximately 70% and 30% on average, respectively). The largest vegetated areas in the three maps were occupied by *Grassland* (about 40% on average) and *Scrubland* (about 26% on average). *Active Dune* and *Reg* classes were the next most common in the three classifications,

Table 5. Proportional vegetation/landform units extent as total hectares and percentage for the study area.

	ASTER		Textural data		ASTER combined texture	
	Hectares	%	Hectares	%	Hectares	%
AD	39	12.6	34	11.0	40	12.9
Reg	51	12.5	56	18.1	51	16.5
Grassland	122	39.4	125	40.3	117	37.7
GSD	11	3.5	8	2.6	14	4.5
Scrubland	84	27.1	81	26.1	78	25.2
SSD	3	1.0	6	1.9	10	3.2

AD, Active Dune; GSD, Grass Stabilized Lineal Dune; SSD, Scrub Stabilized Lineal Dune.

covering approximately 12% and 17% of the area, respectively. It is interesting to note that the main difference between the maps obtained using single datasets *versus* the ASTER combining Radarsat-derived texture map is the proportion of stabilized lineal dunes (4.5% on average *vs*. 7.7%, respectively). Similarly, the vegetated sand sheets area estimation on this map was about 3% lower than the results obtained on the maps using single datasets.

3.3 *Validation*

Accuracy assessments performed for ASTER alone, Radarsat-derived textural information and ASTER combined texture maps are presented in table 6. Overall accuracies of vegetation and landform patterns in these classification outputs were 82.8%, 84.3% and 89.7%, respectively. Table 7 presents the KHAT statistic and its variance, and the Z statistic used for determining whether the classification was significantly better than a random result. At the 95% confidence level, the critical value was 1.96. The Z statistic for the three maps was larger than the critical value and therefore the classifications are significantly better than random.

3.3.1 ASTER data classification. Producer's and user's accuracies for the *Active Dune* class were acceptable (approximately 91% and 95%, respectively; table 6(*a*)) for the ASTER map. This result is expected because this class is easily separable due to its high reflectivity. The observation that active sand surfaces have a higher albedo (are spectrally brighter) than inactive sand surfaces has been made previously (Blount 1988, Blount *et al.* 1990). This yields a high contrast between these areas, making their discrimination possible by thresholding the intensity (Paisley *et al.* 1991).

The *Reg* class presented a producer's accuracy of about 87% and user's accuracy of approximately 77%. The main error of commission (about 13%) for *Reg* was due to confusion with the *Active Dune* class. This confusion is indicative of a sediment availability continuum, where regs and active dunes are areas of low and high sediment availability, respectively. Many of the pixels classified erroneously in the regs were at intermediate positions along this continuum. By contrast, regs could be accurately discriminated from active dunes in the ends of this continuum, possibly because of their lower brightness values. The low reflectance of regs is attributed to the dark colouring of clasts and rock fragments, which cast shadows, trapping more of the incoming sunlight and reducing the amount of reflected energy (Metternicht and Zinck 1998).

The lowest producer's accuracy was obtained for stabilized lineal dunes. However, although considerable confusion occurred between *Grassland* and *GSD* classes (producer's accuracy of approximately 78%), lineal dunes were more accurately identified in the grassland than in the scrubland. The *SSD* class had the lowest producer's accuracy (about 70%) and was mainly confused with the scrubland matrix, which in turn decreased the reliability of this class. A large number of pixels from the *SSD* class were incorrectly included as part of the *Scrubland* (216 out of 567 total pixels). Although this misclassification did not affect the proportion of correctly identified *Scrubland* pixels (333 out of 360), it did decrease the user's accuracy of the *Scrubland* class. The reliability was decreased because as the total number of pixels classified as *Scrubland* features increased, the correctly identified *Scrubland* pixels occupied an increasingly lower proportion of the total (333 out of 567) pixels. This resulted in a much larger *Scrubland* area than

Table 6. Contingency matrix for the accuracy assessment of the object-oriented classifications.

Class	AD	Reg	Grassland	GSD	Scrubland	SSD
(*a*) *ASTER data input*						
AD	666 **(94.87)** ***(91.36)***	36 (5.13) *(8.70)*	0 (0) *(0)*	0 (0) *(0)*	0 (0) *(0)*	0 (0) *(0)*
Reg	63 (13.46) *(8.64)*	360 **(76.92)** *(86.96)*	0 (0) *(0)*	27 (5.77) *(3.23)*	0 (0) *(0)*	18 (3.85) *(2.27)*
Grassland	0 (0) *(0)*	0 (0) *(0)*	324 **(67.92)** *(87.80)*	153 (32.08) *(18.28)*	0 (0) *(0)*	0 (0) *(0)*
GSD	0 (0) *(0)*	0 (0) *(0)*	45 (6.41) *(12.20)*	657 **(93.59)** *(78.49)*	0 (0) *(0)*	0 (0) *(0)*
Scrubland	0 (0) *(0)*	18 (3.17) *(4.35)*	0 (0) *(0)*	0 (0) *(0)*	333 **(58.73)** *(92.50)*	216 (38.10) *(27.27)*
SSD	0 (0) *(0)*	0 (0) *(0)*	0 (0) *(0)*	0 (0) *(0)*	27 (4.62) *(7.50)*	558 **(95.38)** *(70.45)*
(*b*) *Radarsat-derived texture data input*						
AD	630 **(97.22)** *(86.42)*	18 (2.78) *(4.35)*	0 (0) *(0)*	0 (0) *(0)*	0 (0) *(0)*	0 (0) *(0)*
Reg	90 (18.87) *(12.35)*	387 **(81.13)** *(93.48)*	0 (0) *(0)*	0 (0) *(0)*	0 (0) *(0)*	0 (0) *(0)*
Grassland	9 (1.61) *(1.23)*	0 (0) *(0)*	324 **(58.06)** *(87.80)*	225 (40.32) *(26.88)*	0 (0) *(0)*	0 (0) *(0)*
GSD	0 (0) *(0)*	0 (0) *(0)*	45 (6.85) *(12.20)*	612**(93.15)** *(73.12)*	0 (0) *(0)*	0 (0) *(0)*
Scrubland	0 (0) *(0)*	9 (10.00) *(10.87)*	0 (0) *(0)*	0 (0) *(0)*	324 **(72.00)** *(90.00)*	117 (10.00) *(5.68)*
SSD	0 (0) *(0)*	0 (0) *(0)*	0 (0) *(0)*	0 (0) *(0)*	36 (5.06) *(10.00)*	675 **(94.94)** *(85.23)*
(*c*) *ASTER combined textural data input*						
AD	684 **(95.00)** *(93.83)*	36 (5.00) *(8.70)*	0 (0) *(0)*	0 (0) *(0)*	0 (0) *(0)*	0 (0) *(0)*
Reg	45 (7.84) *(4.94)*	378 **(82.35)** *(91.30)*	0 (0) *(0)*	18 (7.84) *(4.30)*	0 (0) *(0)*	18 (7.84) *(4.55)*
Grassland	0 (0) *(0)*	0 (0) *(0)*	306 **(77.27)** *(82.93)*	90 (22.73) *(10.75)*	0 (0) *(0)*	0 (0) *(0)*
GSD	0 (0) *(0)*	0 (0) *(0)*	63 (7.95) *(17.07)*	729 **(92.05)** *(87.10)*	0 (0) *(0)*	0 (0) *(0)*
Scrubland	0 (0) *(0)*	0 (0) *(0)*	0 (0) *(0)*	0 (0) *(0)*	342 **(82.61)** *(95.00)*	72 (17.39) *(9.09)*
SSD	0 (0) *(0)*	0 (0) *(0)*	0 (0) *(0)*	0 (0) *(0)*	18 (2.50) *(5.00)*	702 **(97.50)** *(88.64)*

AD, Active Dune; GSD, Grass Stabilized Lineal Dune; SSD, Scrub Stabilized Lineal Dune.
The diagonals are pixels classified correctly, with user's accuracy (**in parentheses bold**) and producer's accuracy (***in parentheses bold italics***) for each class. User's accuracy shows the error of commission and producer's accuracy shows the error of omission. Non-diagonals represent errors with commission percentage (in parentheses) and omission percentage (*in parentheses and italics*).

Table 7. KHAT statistics, standard errors and *Z* values for the ASTER, textural and ASTER combined texture maps.

Data input	KHAT	Standard error	*Z*
B1–4 ASTER	0.791	0.0077	103.34
Textural measures	0.81	0.0074	105.38
ASTER combined texture	0.874	0.0062	111.19

should have been present within the classification. The producer's accuracy of the *SSD* class decreased as well, as a number of pixels that should have been included within of this class were removed and instead classified as *Scrubland* (27% of the *SSD* truth pixels), thus increasing the *SSD* errors of omission.

The low producer's accuracy for the *SSD* class is probably due to the higher reflectance of the scrubland compared with the grassland, which may have masked the surface expression of the lineal dunes in the ASTER image, limiting the capacity of this sensor to accurately discriminate them. There are two possible reasons for the higher reflectance of the scrubland. First, the presence of dense, white pubescent foliage in *Hyalix argentea* specie dominant in the scrubland (Cabrera 1971). Leaf hairs are common features in desert vegetation, acting to reduce leaf absorption in the visible, which decreases the red edge in many of these plants (Okin and Roberts 2004). Thus, leaf pubescence can have significant effects on leaf spectral characteristics, resulting in an increase of the reflectance, especially in the visible (Ehleringer and Mooney 1978). The second reason for the higher albedo in scrubland is the higher woody biomass (scrubs are more robust, have greater leaf biomass and larger stem diameter than grasses), which would be accompanied by an increment in the amount of reflectance.

3.3.2 Textural data classification. Textural measures were relatively successful in accurately mapping active dunes and regs, but provided less encouraging results in the separation of lineal dunes from the vegetation matrix (table 6(*b*)). *Active Dune* was the class showing the best separation, with producer's and user's accuracies of around 86% and 97%, respectively. The distinctive textural pattern of active dunes with respect to the other covers enabled better discrimination (figure 6). The smooth surface of the active dunes tended to backscatter low energy because the sand behaves more like a specular surface, where the energy of the incident wave is reflected away from the antenna. Blom and Elachi (1981) and Lancaster *et al.* (1992) were also able to discriminate between stabilized and active sand dunes on the basis of their different signal return. The *Reg* class accuracy was also acceptable (producer's and user's accuracies of about 93% and 81%, respectively), although there was some confusion between regs and actives dunes. As discussed in section 3.3.1, many of these errors may be attributed to inadequate sampling.

Grass and *Scrub Stabilized Lineal Dunes* (*GSD* and *SSD*, respectively) were the most representative classes of the confusion associated within the classification of the Radarsat-derived textural dataset. True pixels of *SSD* were misclassified as the *Scrubland* class (approximately 15% of omission errors) and areas of scrubland were classified as lineal dunes (about 5% of commission errors). However, the misclassification of *GSD* was observed to be highest, with a producer's accuracy of about 73%, indicating a high degree of errors of omission. A large number of *Grassland* pixels (225) were incorrectly classified as *GSD*, accounting for

approximately 27% of the actual *GSD*. Accordingly, the *Grassland* class has the lowest user's accuracy (about 58%), indicating a high degree of errors of commission.

The confusion associated with the lineal dunes could be due to the orientation of these features with respect to the radar look direction. The backscatter from dune surfaces is largely controlled by dune topography and incidence angle, except where the vegetation masks the ground return (Blom and Elachi 1981, 1987). Lineal dunes have directional features and so must be oriented approximately perpendicular to the radar beam, otherwise no backscatter will occur (Blom and Elachi 1987, Qong 2000). The look angle of the Radarsat image used in this study was about 44°. If a dune was to be imaged at a look direction of 90° (relative to the dune slip face, which has a slope of approximately 30°) and a look angle of 44°, the local incidence angle would be about 14°. The 30° slope was chosen because this is the angle of repose of sand (Blom 1988, Lancaster 1995) and therefore an active dune would have a slip face approaching this slope. In the case shown here, the flight azimuth was 223° (look direction=133°) and the lineal dunes orientation approximately 100°. Therefore, there were only 33° between the look direction and the dune orientation. Consequently, the local incidence angle was much greater than 14°, eliminating any enhancement of the dunes by topographic effects. Hence, the backscattering of the lineal dunes cannot be attributed to topography in this case, but to the vegetation stabilizing them.

The backscattering from vegetation is mainly determined by the volume scattering, which in turn depends on the size of canopy structural elements relative to the radar wavelength (Ferrazzoli and Guerriero 1995). Therefore, the better discrimination of lineal dunes stabilized by grassland as compared to those vegetated by scrubland may rely on the difference in structure of grasses *versus* the structure of the *Hyalis argentea*, the dominant species on the scrubland. Modelling of volume scattering by randomly oriented canopies indicates that backscattering in the C-band is optimally sensitive to vegetation elements with diameters of less than 0.8 cm (Ferrazzoli and Guerriero 1995). As the diameter decreases below the optimum, the elements became increasingly transparent. The leaves and stems of the grasses in the study area are generally less than 0.5 cm in diameter (Nicora 1978) and would therefore have been transparent, or nearly so, in the C-band. The *Hyalis* sp. canopies contain many stems with diameter larger than 1 cm (Cabrera 1971) and would therefore be expected to contribute strongly to the backscatter of the C-band signal. In addition, scrubs are taller and their leaves are longer than grasses, contributing to the higher backscatter of the *Hyalis* sp. stands. Hence, the higher classification accuracies of the *SSD* class, as compared to the *GSD* class, could be attributed to the increased roughness, and thus coarser texture, of the scrubland relative to the grassland, therefore enabling better discrimination of lineal dunes stabilized by scrub.

3.3.3 ASTER combined Radarsat textural data classification. The map resulting from the object-oriented classification using spectral and textural data inputs shows high overall accuracy and kappa statistic (89.7% and 87.4%, respectively), as well as high producer's and user's accuracy for all the classes, excepting the *Grassland* class (table 6(*c*)). This means that most of the vegetation and landform patterns have been correctly identified, with low omission and commission errors. The *Grassland* class had the lowest user's accuracy (about 77%), the main error being commission for this class the confusion with the *GSD* class (approximately 23%). This

Table 8. Kappa analysis result for the pairwise comparison of error matrices.

Pairwise comparison	*Z*
ASTER *vs.* ASTER combined texture	5.96
Textural data *vs.* ASTER combined texture	4.69

misclassification could be attributed to the spectral and textural similarity of these classes, as discussed previously.

3.4 *Efficiency of the synergistic approach*

3.4.1 From a classification accuracy perspective. The *Z* score of the kappa analysis for the pairwise comparison between the ASTER-derived and the combination of ASTER and Radarsat-derived textural information (table 8) shows a result of 5.96, which is superior to 1.96 (the critical value at the 95% confidence level), indicating that the two error matrices are significantly different. Table 8 summarizes the kappa analysis results for the pairwise comparison of the textural data and ASTER combined texture error matrices. The result (4.69) is again greater than 1.96, suggesting that the two matrices are significantly different. A comparison of the classification accuracies obtained with the different layer combinations revealed that the ASTER combined texture had better overall accuracy (89.7%) and a higher KHAT statistic value (87.4%) than the classifications resulting from the use of single optical (82.8% and 79.1%, respectively) or textural (84.3% and 81.0%, respectively) layer input, indicating that the synergic approach enabled better discrimination of vegetation and landform patterns in the study area.

Classification outputs using ASTER alone and textural information were compared with the ASTER combined texture output using a fuzzy approach, to produce maps of spatial agreement (figure 8). Areas of agreement show values close

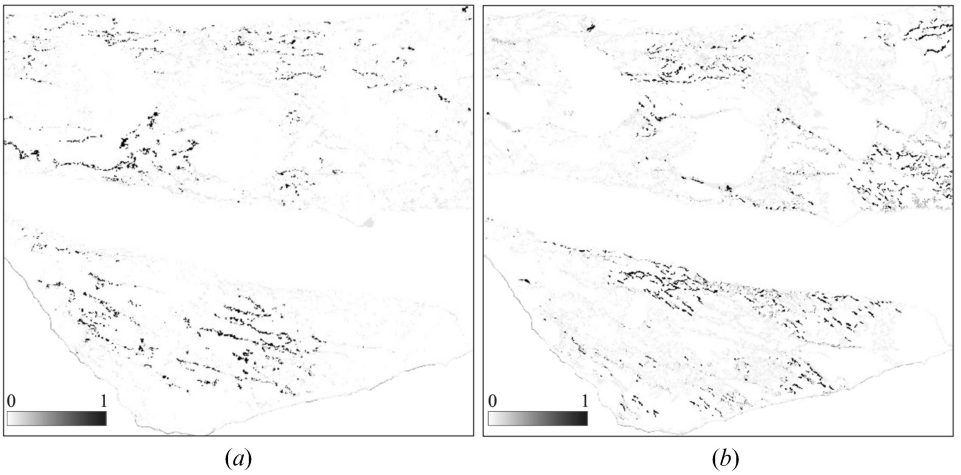

(*a*) (*b*)

Figure 8. Spatial assessment of similarity using the two-way fuzzy map comparison: (*a*) ASTER data input *vs*. ASTER combined texture information classifications, and (*b*) textural measures *vs*. ASTER combined texture data classifications. Areas mapped identically have values close to or equal to 0, while areas of total disagreement show values close to or equal to 1.

to zero, while areas of total disagreement on class assignation take a value close to or equal to one. Figure 8(*a*), which compares ASTER *versus* the synergy of ASTER and texture layers, shows that the highest disagreement appeared in scrubland areas, where the synergy of ASTER and texture layers classified lineal dunes, while the ASTER data classified most of these same areas as *Scrubland* class. Additionally, figure 8(*a*) reveals a strong agreement in the spatial classification of the *Active Dune* and *Reg* classes.

By contrast, the areas recording the highest disagreements between textural and ASTER combined texture maps tend to correspond to grassland extents (figure 8(*b*)). There are large areas classified as lineal dunes in the ASTER combined texture map, but these appear as the *Grassland* class in the textural map. Furthermore, figure 8(*b*) reveals that, as with the comparison between ASTER and ASTER combined texture maps, there is strong agreement between the classifications of active dunes and regs.

3.4.2 Economic/financial point of view. Classification accuracy itself may not be the sole criterion determining the choice of the sensor/s to mapping vegetation/ landforms. Image cost is obviously important. The synergic use of ASTER and textural datasets is more expensive, hence a cost-effectiveness analysis is necessary to evaluate it. The results of this study (figure 9) show that active dunes mapped from single ASTER or Radarsat datasets achieved a level of classification accuracy that was almost as high as that derived from the use of ASTER combining texture information. Therefore, to map active dunes a single sensor may be used, without significant loss of accuracy and with a substantially lower cost. By contrast, the synergic use of ASTER and Radarsat to mapping lineal dunes stabilized by vegetation significantly improved the level of classification accuracy, and is thus a cost-effective alternative to map these features.

4. Conclusions

This paper has presented a detailed evaluation of the use of remote sensing data in the visible, NIR and microwave parts of the spectrum to map vegetation and

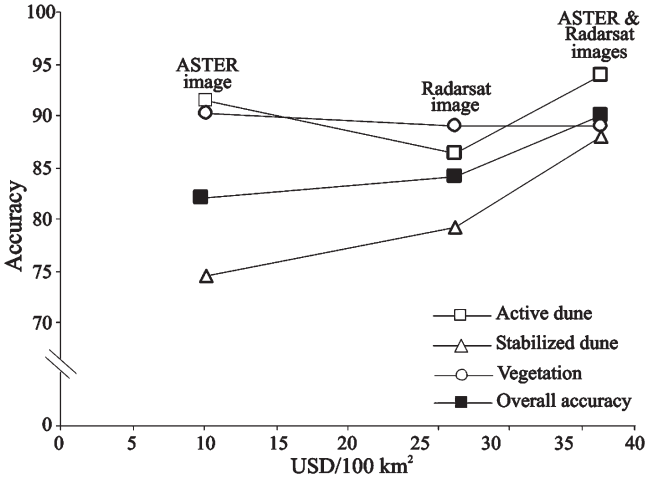

Figure 9. Accuracies *vs.* image cost. Image prices: ASTER scene=USD 10.10/100 km^2, RADARSAT scene=USD 27.50/100 km^2.

landform patterns in a sandy rangeland. The proposed data processing procedure integrated textural analysis of Radarsat-SAR data and Terra-ASTER VNIR data. The analysis was performed using an object-oriented classifier. We have shown that a thematic classification from the synergy of ASTER and Radarsat-derived texture data had better overall accuracy and a higher KHAT statistic value than the classifications resulting from single sensor data inputs. The study shows that the two types of sensors, ASTER and Radarsat, provide different information and can be effectively used to map vegetation/landform classes in Peninsula Valdés, Patagonia, Argentina. The following conclusions may be drawn from this study.

The original radar data present poor effectiveness in visual delineation of vegetation and landform patterns. Radarsat-derived textural measures based on the GLC matrix approach were used to increase the discriminatory ability of the original SAR image. Haralick's textural features, namely mean, variance, dissimilarity (all computed at IPD=5) and contrast (computed at IPD=7)), as optimized with this approach, appear to be the best textural features to improve interclass discrimination.

The *Active Dune* and *Reg* classes were identified as the dominant landforms in all classifications at 12% and 17% coverage, respectively. The stabilized lineal dunes comprised a larger proportion of the surface area in the combined ASTER and Radarsat-derived texture map, than in the single dataset maps (7.7% *vs*. 4.5% on average, respectively). Areas dominated by sandsheets occupied 3% more surface in the maps using ASTER and textural measures datasets alone, in comparison with the map obtained from optical and Radarsat-derived texture data.

The results of the accuracy and map comparison suggested that the two types of sensors, ASTER and Radarsat, provide information on different aspects and have potential for complementarity. Both sensors were relatively successful in accurately mapping active dunes and regs but experienced difficulties in the discrimination of lineal dunes from the vegetation matrix. In contrast to ASTER, lineal dunes could be more accurately discriminated from the scrubland using Radarsat-derived textural data but, unlike ASTER, lineal dunes could not be accurately distinguished from the grassland using textural measures derived from radar. Vegetation type influenced VNIR reflectance and radar backscatter. Native grasses had low radar backscatter as well as low VIR reflectance. *Hyalis argentea*, the dominant scrub specie, had high values for both sensor groups. Other features, such as active dunes, had high values for VNIR and low radar backscatter, while desert pavements or reg characterized by high rock fragment content and strong microtopography had high radar backscatter but low VIR reflectance.

The object-based classification technique used in this study proved a valuable tool and was suitable for optical and radar data classification. Objects with similar spectral reflectance and radar backscatter, such as stabilized lineal dunes, could be discriminated by describing differences between neighbouring objects as well as objects on a different hierarchical level. In addition, the object-oriented classifier allowed interpretation of each decision rule and made efficient use of only important objects' features for the classification. Future related research will include the application of the technique over larger areas; comparison with other classifiers, including neural networks and decision trees approaches; further evaluation of different radar angles and look directions; and analysis of the influence of image date on the approach proposed in this study.

Acknowledgements

We acknowledge the valuable suggestions made by two anonymous reviewers and by Diego Giberto, which greatly improved the manuscript. This study was funded by CONICET (PIP-2004, No. 6413) and FONCyT (BID 1728/OC-AR PICTR/03 No. 439). Comisión Nacional de Actividades Espaciales (CONAE) supplied the Terra-ASTER and Radarsat-1 ASAR images within the framework of the project to promote monitoring of World Heritage sites (UNESCO). We thank Walter Sione (PRODITEL-Universidad Nacional de Lujan) for facilitating the eCognition software, and the Department of Spatial Sciences, Curtin University of Technology, where the leading author spent three months in research.

References

ANYS, H. and HE, D.C., 1995, Evaluation of textural and multipolarization radar features for crop classification. *IEEE Transactions on Geoscience* and *Remote Sensing*, **33**, pp. 1170–1181.

BAATZ, M., BENZ, U., DEHGHANI, S., HEYNEN, M., HLTJE, A., HOFMANN, P., LINGENFELDER, I., MIMLER, M., SOHLBACH, M., WEBER, M. and WILLHAUCK, G., 2004, *eCognition Professional: User Guide 4* (Munich: Definiens-Imaging).

BAATZ, M. and SCHAEPE, A., 2000, Multiresolution segmentation: an optimization approach for high quality multi-scale image segmentation. In *Angewandte Geographische Informationsverarbeitung (AGIT, Applied Geographic Information Processing)*, J. Strobl and T. Blaschke (Eds), pp. 12–23 (Heidelberg: Wichmann-Verlag).

BAHRE, C.J. and SHELTON, M.L., 1993, Historic vegetation change, mesquite increases, and climate in southeastern Arizona. *Journal of Biogeography*, **20**, pp. 489–504.

BALLANTINE, J.A.C., OKIN, G.S., PRENTISS, D.E. and ROBERTS, D.A., 2005, Mapping North African landforms using continental-scale unmixing of MODIS imagery. *Remote Sensing of Environment*, **47**, pp. 470–483.

BARROS, V.R. and RIVERO, M., 1982, *Mapas de Probabilidad de la Precipitación en la Provincia de Chubut (Precipitation Probability Maps in Chubut Province). Contribución 54* (Puerto Madryn, Argentina: CENPAT-CONICET).

BARROS, V.R., RIVERO, M., RODRIGUEZ SERÓ, J.A. and LABRAGA, J.C., 1981, *Primeras Jornadas de Energía Eólica (First Workshop of Aeolian Energy). Contribución 56* (Puerto Madryn, Argentina: CENPAT-CONICET).

BELTRAMONE, C., VILLEGAS, M. and DEMICHELIS, A., 1993, Depósitos eólicos del sur de Península Valdés, Chubut (Aeolian deposits in the South of Valdes Peninsula). In *III Reunión Argentina de Sedimentología*, 20–24 May 1993, San Juan, Argentina (La Plata, Argentina: AAS), pp. 360–365.

BENZ, U.C., HOFFMANN, P., WILLHAUCK, G., LINGENFELDER, I. and HEYNEN, M., 2004, Multi-resolution, object-oriented fuzzy analysis of remote sensing data for GIS-ready information. *ISPRS Journal of Photogrammetry and Remote Sensing*, **58**, pp. 239–258.

BERTILLER, M.B., BEESKOW, A.M. and IRISARRI, M.P., 1981, *Caracteres fisonómicos y florísticos de vegetación del Chubut: La Península Valdés y el Istmo Ameghino (Vegetation Physiognomy in Chubut: Valdes Peninsula and Ameghino Isthmus). Contribución 41* (Puerto Madryn, Argentina: CENPAT-CONICET).

BLOM, R.G., 1988, Effects of variation in look angle and wavelength in radar images of volcanic and aeolian terrains, or now you see it, now you don't. *International Journal of Remote Sensing*, **9**, pp. 945–965.

BLOM, R. and ELACHI, C., 1981, Spaceborne and airborne imaging radar observation of sand dunes. *Journal of Geophysical Research*, **86**, pp. 3061–3073.

BLOM, R. and ELACHI, C., 1987, Multifrequency and multipolarization radar scatterometry of sand dunes and comparison with spaceborne and airborne radar images. *Journal of Geophysical Research*, **92**, pp. 7877–7889.

BLOUNT, H.G., 1988, Regional aeolian dynamics from remote sensing: origin of the Gran Desierto, Sonora, México. PhD thesis, Arizona State University.

BLOUNT, H.G., SMITH, M.O., ADAMS, J.B., GREELEY, R. and CHRISTENSEN, P.R., 1990, Regional aeolian dynamics and sand mixing in the Gran Desierto: evidence from Landsat Thematic Mapper images. *Journal of Geophysical Research*, **95**, pp. 15463–15482.

BLUMBERG, D.G., 1998, Remote sensing of desert dune forms by polarimetric synthetic aperture radar (SAR). *Remote Sensing of Environment*, **65**, pp. 204–216.

CABRERA, A.L., 1971, Compositae. Parte VII. In *Flora Patagonica (Pantagonian Flora). Tomo VIII*, M.N. Correa (Ed.), p. 451 (Buenos Aires, Argentina: INTA).

COHEN, J., 1960, A coefficient of agreement for nominal scales. *Educational and Psychological Measurement*, **1**, pp. 37–40.

CONGALTON, R., 1991, A review of assessing the accuracy of classifications of remotely sensed data. *Remote Sensing of Environment*, **37**, pp. 35–46.

CONGALTON, R.G. and GREEN, K., 1999, *Assessing the Accuracy of Remotely Sensed Data: Principles and Practices* (New York: Lewis).

CORONATO, F.R., 1994, Clima del Nordeste del Chubut (Northeastern Chubut Climate). In *CADINQUA*, A. Súnico, P. Bouza, C. Cano, H. del Valle, L. Videla and A. Monti (Eds), pp. 13–20 (Puerto Madryn, Argentina: Cenpat-CONICET).

DEFINIENS, 2003, *eCognition User Guide version 4.0*. Available online at: www.definiens-imaging.com/.

DEFOSSÉ, G.E., BERTILLER, M.B. and ROSTAGNO, C.M., 1992, Rangeland management in Patagonian drylands. In *Proceedings of the International Rangeland Development Symposium*, G.K. Perrier and C.W. Gay (Eds), pp. 12–21 (Spokane, WA: Society for Range Management).

DEL VALLE, H.F. and BLANCO, P.D., 2006, Indicadores espectrales del rango de las microondas para la evaluación y monitoreo de la erosión eólica (Aeolian erosion evaluation and monitoring using indictors in the microwave spectral range). In *Indicadores de la desertificación para América del Sur (Desertification Indicators for South America)*, E.M. Abraham and G. Beekman (Eds), pp. 65–84 (Mendoza: BID-IICA).

DEL VALLE, H.F., ROSTAGNO, C.M., CORONATO, F.R., BOUZA, P.J. and BLANCO, P.D., 2007, Sand dune activity in north-eastern Patagonia. *Journal of Arid Environments*, **72**, pp. 411–422.

DRAGUT, L. and BLASCHKE, T., 2006, Automated classification of landform elements using object-based image analysis. *Geomorphology*, **81**, pp. 330–344.

EHLERINGER, J.R. and MOONEY, H.A., 1978, Leaf hairs: effects on physiological activity and adaptive value to a desert shrub. *Oecologia*, **37**, pp. 183–200.

ELACHI, C., BICKNELL, T., JORDAN, R.L., WU, Ch.L. and WU, Ch., 1982, Spaceborne synthetic-aperture imaging radars: applications, techniques and technology. *Proceedings of the IEEE*, **10**, pp. 1174–1209.

ERDAS INC., 2003, *ERDAS, Version 8.7*. Available online at: www.erdas.com/.

ERSDAC, 2000, *Advanced Spaceborne Thermal Emission and Reflection Radiometer*. Available online at: http://asterweb.jpl.nasa.gov/ (accessed 9 October 2007).

FERRAZZOLI, P. and GUERRIERO, L., 1995, Radar sensitivity to tree geometry and woody volume: a model analysis. *IEEE Transactions on Geoscience* and *Remote Sensing*, **33**, pp. 360–371.

FORD, J.P., BLOM, R.G., CRISP, J.A., ELACHI, C., FARR, T.G., SAUNDERS, R.S., THEILIG, E.E., WALL, S.D. and YEWELL, S.B., 1989, *Spaceborne Radar Observations: A Guide for Magellan Radar-Image Analysis* (Pasadena, CA: JPL).

FROHN, R.C., HINKEL, K.M. and EISNER, W.R., 2005, Satellite remote sensing classification of thaw lakes and drained thaw lake basins on the North Slope of Alaska. *Remote Sensing of Environment*, **97**, pp. 116–126.

GREELEY, R. and BLUMBERG, D.G., 1995, Preliminary analysis of Shuttle Radar Laboratory (SRL-1) data to study aeolian features and processes. *IEEE Transactions on Geoscience and Remote Sensing*, **33**, pp. 927–932.

HAACK, B. and BECHDOL, M., 2000, Integrating multisensor and RADAR texture measures for land cover mapping. *Computers and Geosciences*, **26**, pp. 411–421.

HAGEN-ZANKER, A., STRAATMAN, B. and ULJEE, I., 2005, Further developments of a fuzzy set map comparison approach. *International Journal of Geographical Information Science*, **19**, pp. 769–785.

HALL-BEYER, M., 2004, *GLCM Texture: A Tutorial Version 2.10*. Available online at: www.fp.ucalgary.ca/mhallbey/tutorial.htm (accessed 9 October 2007).

HARALICK, R.M., 1979, Statistical and structural approaches to texture. *Proceedings of the IEEE*, **67**, pp. 786–803.

HARALICK, R.M., SHANMUGAN, K.S. and DINSTEIN, I., 1973, Textural features for image classification. *IEEE Transactions on Systems, Man and Cybernetics*, **3**, pp. 610–621.

HEROLD, N., HAACK, B. and SOLOMON, E., 2004, An evaluation of radar texture for land use/cover extraction in varied landscapes. *International Journal of Applied Earth Observation and Geoinformation*, **5**, pp. 113–128.

HSU, S., 1978, Texture-tone analysis for automated landuse mapping. *Photogrammetric Engineering and Remote Sensing*, **44**, pp. 1393–1404.

HUDAK, A.T. and WESSMAN, C.A., 1998, Textural analysis of historical aerial photography to characterize woody plant encroachment in South African savanna. *Remote Sensing of Environment*, **66**, pp. 317–330.

HUDAK, A.T. and WESSMAN, C.A., 2001, Textural analysis of high resolution imagery to quantify bush encroachment in Makidwe Game Reserve, South Africa, 1955–1996. *International Journal of Remote Sensing*, **22**, pp. 2731–2740.

HUETE, A.R., 1988, A soil-adjusted vegetation index (SAVI). *Remote Sensing of Environment*, **25**, pp. 295–309.

KARATHANASSI, V., IOSSIFIDIS, C. and ROKOS, D., 2000, A texture-based classification method for classifying built areas according to their density. *International Journal of Remote Sensing*, **21**, pp. 1807–1823.

KURVONEN, L. and HALLIKAINEN, M.T., 1999, Textural information of multitemporal ERS-1 and JERS-1 SAR images with applications to land and forest type classification in boreal zone. *IEEE Transactions on Geoscience and Remote Sensing*, **37**, pp. 680–689.

KUTIEL, P., COHEN, O. and SHOSHANY, M., 2004, Vegetation establishment on the southern Israeli coastal sand dunes between the years 1965 and 1999. *Landscape and Urban Planning*, **67**, pp. 141–156.

LABRAGA, J.C., 1994, On extreme winds in Pampa del Castillo Plateau, Patagonia Argentina, with reference to wind farm settlement. *Journal of Applied Meteorology*, **33**, pp. 85–95.

LANCASTER, N., 1995, *Geomorphology of Desert Dunes* (London: Routledge).

LANCASTER, N., GADDIS, L. and GREELEY, R., 1992, New airborne imaging radar observations of sand dunes: Kelso dunes, California. *Remote Sensing of Environment*, **39**, pp. 233–238.

LE HOUÉROU, H.N., 1993, An overview of desertisation in world arid lands. In *Illustrated Library of the Earth: Deserts*, M.K. Seely (Ed.), pp. 1–13 (Sydney: Weldon Owen).

LEE, J.S. and JURKEVICH, I., 1994, Speckle filtering of synthetic aperture radar images: a review. *Remote Sensing Reviews*, **8**, pp. 313–340.

METTERNICHT, G.I. and ZINCK, J.A., 1998, Evaluating the information content of JERS-1 SAR and Landsat TM data for discrimination of soil erosion features. *ISPRS Journal of Photogrammetry and Remote Sensing*, **53**, pp. 143–153.

MILCHUNAS, D.G. and LAUENROTH, W.K., 1993, Quantitative effects of grazing on vegetation and soil over a global range of environments. *Ecological Monographs*, **63**, pp. 327–366.

NARASIMHA RAO, P.V., SESHA SAI, M.V.R., SREENIVAS, K., KRISHNA RAO, M.V., RAO, B.R.M., DWIDEDI, R.S. and VENKATARATNAM, L., 2002, Textural analysis of

IRS-1D panchromatic data for land cover classification. *International Journal of Remote Sensing*, **23**, pp. 3327–3345.

NICORA, E.G., 1978, Graminae. Parte III. In *Flora Patagonica (Pantagonian Flora). Tomo VIII*, M.N. Correa (Ed.), p. 563 (Buenos Aires, Argentina: INTA).

OIES, 1991, *Arid Ecosystem Interactions* (Boulder, CO: Office of Interdisciplinary Earth Studios).

OKIN, G.S., MURRAY, B. and SCHLESINGER, W.H., 2001, Degradation of sandy arid shrubland environments: observations, process modeling, and management implications. *Journal of Arid Environments*, **47**, pp. 123–144.

OKIN, G.S. and ROBERTS, D.A., 2004, Remote sensing in arid regions: challenges and opportunities. In *Manual of Remote Sensing*, S. Ustin (Ed.), p. 15 (New York: John Wiley and Sons).

PAISLEY, E.C.I., LANCASTER, N., GADDIS, L.R. and GREELYE, R., 1991, Discrimination of active and inactive sand from remote sensing: Kelso dunes, Mojave desert, California. *Remote Sensing of Environment*, **37**, pp. 153–166.

PALMER, A.R. and VAN ROOYEN, A.F., 1998, Detecting vegetation change in the southern Kalahari using Landsat TM data. *Journal of Arid Environments*, **39**, pp. 143–153.

PERKINS, J.S. and THOMAS, D.S.G., 1993, Spreading deserts or spatially confined environmental impacts? Land degradation and cattle ranching in the Kalahari Desert of Botswana. *Land Degradation and Rehabilitation*, **4**, pp. 179–194.

QONG, M., 2000, Sand dune attributes estimated from SAR images. *Remote Sensing of Environment*, **74**, pp. 217–228.

RYHERD, S. and WOODCOCK, C.E., 1996, Combining spectral and texture data in the segmentation of remotely sensed images. *Photogrammetric Engineering and Remote Sensing*, **62**, pp. 181–194.

SANJEEVI, S., 1996, Morphology of dunes of the Coromandel coast of Tamil Nadu: a satellite based approach for coastal landuse planning. *Landscape and Urban Planning*, **34**, pp. 189–195.

SANO, E.E., QI, J., HUETE, A.R. and MORAN, M.S., 1998, The use of SAR/TM synergy for estimating soil moisture content over a semi-arid rangeland. *Proceedings of the Second Latino-American Seminar on Radar Remote Sensing*, 11–12 September, Santos, Sao Paulo, Brazil (Noordwijk, The Netherlands: ESA) SP–343, on CD-ROM.

SCHIEWE, J., TUFTE, L. and EHLERS, M., 2001, Potential and problems of multi-scale segmentation methods in remote sensing. *GeoBIT/GIS*, **6**, pp. 34–39.

SCHLESINGER, W.H., REYNOLDS, J.F., CUNNINGHAM, G.L., HUENKE, L.F., JARRELL, W.M., VIRGINIA, R.A. and WHITFORD, W.G., 1990, Biological feedbacks in global desertification. *Science*, **247**, pp. 1043–1048.

SHUPE, S. and MARSH, S.E., 2004, Cover and density based vegetation classifications of the Sonoran desert using Landsat TM and ERS-1 SAR imagery. *Remote Sensing of Environment*, **93**, pp. 131–149.

STAFFORD SMITH, D.M., 1996, Management of rangelands: paradigms at their limits. In *The Ecology and Management of Grazing Systems*, J. Hodgson and A.W. Illius (Eds), pp. 325–357 (Wallingford, UK: CABI).

STORY, M. and CONGALTON, R., 1986, Accuracy assessment: a user's perspective. *Photogrammetric Engineering and Remote Sensing*, **52**, pp. 397–399.

SÚNICO, A., 1996, Geología del cuaternario y Ciencia del Suelo: Relaciones geomórficas-estratigráficas con suelos y paleosuelos (Quaternary Geology and Soil Science: Geomorphic-stratigraphic relations with soils and paleosoils). PhD thesis, Universidad Nacional de Buenos Aires.

THOMAS, N., HENDRIX, C. and CONGALTON, R.G., 2003, A comparison of urban mapping methods using high-resolution digital imagery. *Photogrammetric Engineering and Remote Sensing*, **69**, pp. 963–972.

TREITZ, P. and HOWARTH, P., 2000, Integrating spectral, spatial, and terrain variables for forest ecosystem classification. *Photogrammetric Engineering and Remote Sensing*, **66**, pp. 305–317.

TUCKER, C.J., DREGNE, H.E. and NEWCOMB, W.W., 1991, Expansion and contraction of the Sahara desert from 1980 to 1990. *Science*, **253**, pp. 299–301.

TUCKER, C.J., NEWCOMB, W.W. and DREGNE, H.E., 1994, AVHRR data sets for determination of desert spatial extent. *International Journal of Remote Sensing*, **15**, pp. 3547–3565.

ULABY, F., KOUYATE, F., BRISCO, B. and WILLIAMS, T.H.L., 1986, Textural information in SAR images. *IEEE Transactions on Goscience and Remote Sensing*, **24**, pp. 35–245.

VAN DER SANDEN, J.J. and HOEKMAN, D.H., 1999, Potential of airborne radar to support the assessment of land cover in a tropical rain forest environment. *Remote Sensing of Environment*, **68**, pp. 26–40.

WARREN, A. and AGNEW, C., 1988, *An Assessment of Desertification and Land Degradation in Arid and Semi-arid Areas.* International Institute for Environment and Development Paper No. 2 (London: IIED, University College).

WESKA, J.C., DYER, R. and ROSENFELD, A., 1976, A comparative study of texture measures for terrain classification. *IEEE Transactions on Systems, Man and Cybernetics*, **6**, pp. 269–285.

WHITFORD, W.G., MARTINEZ, T.G. and MARTINEZ, M.E., 1995, Persistence of desertified ecosystems: explanations and implications. *Environmental Monitoring and Assessment*, **37**, pp. 319–322.